Progress In Electromagnetics Research C, Vol. 130, 155–167, 2023

Miniaturization of Printed Rectangular Monopole Antenna by Using Slots for Triple Band Applications

Alka Khade, Mahadu Trimukhe, Shubhangi Verulkar, and Rajiv K. Gupta*

Abstract—We propose a miniaturized tripleband printed monopole antenna for 5G, WLAN, WiMAX, and X-band applications. Slots are etched in a printed rectangular monopole to design the antenna. A slot etched in a rectangular monopole increases the capacitance and therefore, decreases the resonant frequency or miniaturizes the antenna. Slots in a rectangular monopole antenna also create different current path lengths which resonates at different frequencies. Three slots are etched, and parameters are optimized to achieve triple bands to operate over 5G (3.3 to 3.6 GHz), WiMAX (3.4 to 3.6 GHz), WLAN (5.725–5.875 GHz), WLAN 5.9 GHz band (5.850–5.925 GHz), and X-band (7.3–7.9). The lower 45 MHz (5.850–5.925 GHz) and upper 30 MHz (5.895–5.925 GHz) of WLAN band also find applications for automobile safety in Cellular Vehicle-to-Everything (C-V2X) technology. The radiation patterns are nearly omnidirectional. The antenna is fabricated on a $0.154\lambda_0 \times 0.143\lambda_0$ board area, where λ_0 is the free-space wavelength at 3.3 GHz. The measured results are in close agreement with the simulation ones.

1. INTRODUCTION

Wireless technology has seen tremendous growth, rapid changes, and evolved at a rapid rate from 2G to 5G technology. Besides this, there are numerous services such as Bluetooth, WLAN, Wi-Fi, and WiMAX that support a wireless communication system. The growth and demand of a mobile communication system, which can not only offer improved functionality and enhanced performance but also has small size and available at low cost, is increasing continuously. Conventionally, multiple antennas are required to offer multiple services. However, multiple antennas increase not only the size but also the cost of the system. Therefore, multiband antennas are designed to operate over distinct frequency bands. As a result, researchers are always engaged in the design of compact, low-cost, novel multiband antennas suitable for rapidly developing communication systems.

Traditionally, multiband antenna design involves multiple branches. The length of each branch determines the resonant frequency of a frequency band, while its bandwidth is controlled by the width of the branch. Multiband antennas are designed with branches of different shapes [1, 2]. Meander line and G-shape branches on defective ground are used to miniaturize the size of triple band antenna [1]. Another tri-band antenna using three C-shaped round branches has been reported in which each C-shape independently controls a band [2]. Slots or slits are etched, or stubs are added in ground or radiating element to design a multi-band antenna [3–12]. A multi-band antenna is designed by incorporating Pi-shape and inverted L-shape slots in an asymmetric beveling rectangular patch in [3] whereas two L-shaped stubs and two arc-shaped strips on a partial ground are employed for achieving tri-band operation in [4]. A coplanar waveguide (CPW)-fed tri-band antenna using an open folded stub with two L-shaped strips of different lengths on asymmetric trapezoidal ground is reported in [5]. With the addition of a

Received 24 December 2022, Accepted 16 February 2023, Scheduled 26 February 2023
* Corresponding author: Rajiv Kumar Gupta (rajivgupta@ternaengg.ac.in).
The authors are with the Department of Electronics and Telecommunication, Terna Engineering College, Navi-Mumbai, India.

vertical slot, two horizontal slots, and two hook-shaped branches, a pentagon is transformed into a tri-band antenna [6]. Multiple stubs are incorporated in defective ground to design a multi-band antenna in [7]. A triple band antenna is designed by adding an L-shaped strip to a circular branch in [8]. The coupling between ultra-wideband (UWB) antenna's higher-order modes is reduced to achieve tri-band operation. Two annular-ring slots, two L-shaped and one I-shaped slots are etched in a rectangular patch, and an elliptical-shaped-slit (ESS) is etched in ground to achieve tri-band operation in [9]. U and H shaped slots are incorporated in a rectangular monopole, and a defected ground structure (DGS) with two E shaped and a F-shaped slot is designed to achieve triple bands [10]. A split ring is etched in a rectangular monopole while a U-shaped slot is etched in the ground plane for tri-band operation in [11]. A CPW-fed rectangular monopole antenna is designed on a DGS. A parasitic strip and a Hilbert strip are coupled to monopole to achieve wideband circular polarized (CP) antenna [12].

Meta-material and split ring resonator (SRR) are used in designing multiband antennas [13–16]. A square-shaped slot antenna is designed, and strips and SRR are incorporated to achieve CP tri-band operation [13]. A miniaturized triple-band antenna is designed using a half-split ring and an SRR [14]. An annular ring having eight slots along its periphery is loaded by SRR and a series of octagonal closed rings to design a multiband antenna [15]. A meta-material inspired dual-band antenna consisting of a triangular SRR with an open stub is reported in [16]. An on-glass transparent antenna using two square and hexagon rings is proposed for tri-band operation [17]. The antenna is small in size but uses multiple substrates. A hexagonal SRR (HSRR) with a circular SRR (CSRR) placed inside it is designed and loaded with a double slit HSRR to operate over sub-6 GHz multi-bands [18]. A rectangular monopole is modified into two split rings connected by a common arm to operate as a dual band antenna [19]. Fractal technique is employed to design multiband antennas [20, 21]. Using triangular and circular fractal, a circular nested triangular fractal multiband antenna is reported in [20]. A dual-band antenna is designed using binary branch fractal in [21]. PIN diodes are employed in capacitively loaded slots to achieve reconfigurability in multiband planar inverted F-shape antenna (PIFA) [22]. Using PIN diodes, a multiband frequency reconfigurable antenna on a flexible polyamide substrate consisting of F-shaped and inverted L-shaped monopoles is designed [23]. A spiral-shaped antenna structure is designed, and frequency reconfigurability is achieved using lumped elements in [24]. A dual-band frequency tuneable PIFA antenna is reported in [25] which uses a varactor diode. However, all these antennas have large dimensions.

In this paper, a miniaturized triple-band monopole antenna for 5G, WLAN, WiMAX, and X-band applications is designed by etching slots in a rectangular monopole antenna (RMPA). Slots in rectangular monopole antenna create different current path lengths which resonates at different frequencies. Slots also increase the capacitance and inductance as surface current path length increases, which enables the structure to resonate at a lower frequency and thus, miniaturizes the structure. The prototype antenna is fabricated on a $0.154\lambda_0 \times 0.143\lambda_0$ FR4 substrate. The proposed antenna is novel as it is easy to design. Each slot etched in RMPA generates a band and miniaturizes the antenna. Three slots etched in RMPA provide the desired triple bands and miniaturize the antenna size by 30%. Three bands can be controlled independently. The antenna is low in cost and has smaller dimensions than the reported antennas in the literature.

2. DESIGN THEORY, EVOLUTION STEPS AND ANTENNA GEOMETRY

A slot etched in a rectangular monopole antenna (RMPA) increases the capacitance of the structure and therefore, decreases the resonant frequency or miniaturizes the antenna. A slot etched in the structure where the surface current density is more introduces more capacitance than a slot where the surface current density is less. A slot at the edge also increases the path length and therefore, reduces the resonant frequency and miniaturizes the antenna structure. The increase in conducting path length increases the inductance and decreases the resonant frequency. The increase in inductance also depends on the surface current density. A slot, etched in an RMPA results in the emergence of a band. Three slots are etched to provide the desired triple bands. Each band can be obtained easily by varying the dimensions of a slot resonating over that frequency band.

Figure 1 illustrates the detailed geometry and parameters of the antenna. Three slots are etched at the edge of RMPA to achieve tri-bands, and different parameters are optimized. The optimum

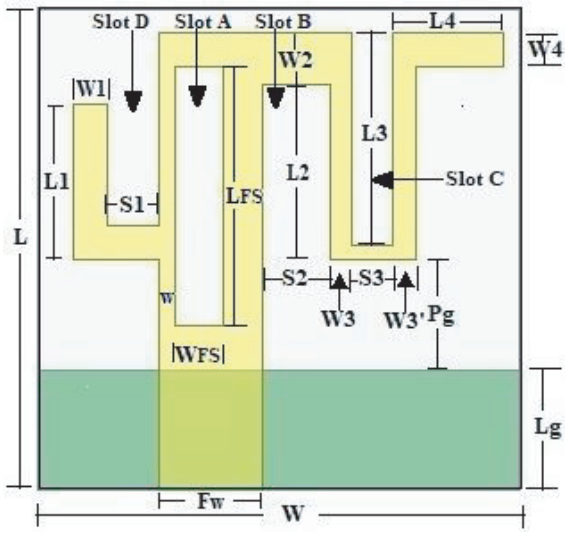

Figure 1. Geometry of the antenna.

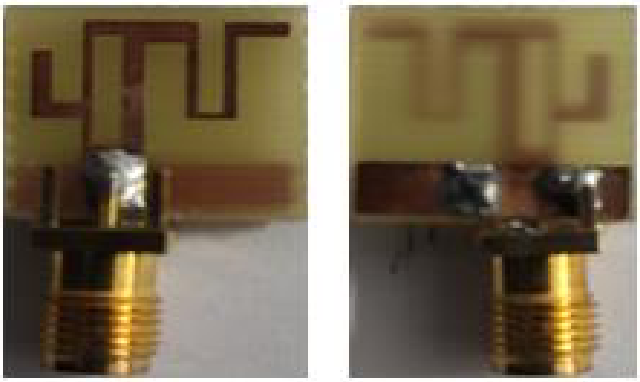

(a) Top view (b) Bottom view

Figure 2. Fabricated prototype antenna.

Table 1. Optimum parameters' dimensions of the antenna.

Parameters	L	W	Lg	Pg	WFS	LFS	W	$S1$	$S2$	$S3$
dimensions (mm)	13	14	3.5	2.5	1.4	7.5	0.5	1.5	2	1.2
Parameters	$L1$	$L2$	$L3$	$L4$	$W1$	$W2$	$W3$	$W3'$	$W4$	Fw
dimensions (mm)	4.5	5.1	6.2	3.2	1	1.5	0.6	0.7	1	3

parameters' dimensions are tabulated in Table 1. 50 Ω microstrip-line fed antenna occupies a $14 \times 13\,\text{mm}^2$ FR4 substrate area (thickness = 1.6 mm, dielectric constant = 4.2 loss tangent =0.02). The simulation and optimization are carried out using HFSS. The fabricated antenna is shown in Fig. 2.

The evolution stages of the proposed antenna are shown in Fig. 3. Initially, $6.6 \times 10\,\text{mm}^2$ RMPA termed as 'Antenna 1' is designed on a $16 \times 14\,\text{mm}^2$ FR4 substrate. The lowest frequency f_L corresponding to $S_{11} = -9.5\,\text{dB}$ (VSWR = 2) of RMPA can be calculated by equating the surface area of RMPA of length L and width W to a cylindrical wire monopole antenna of length L and radius

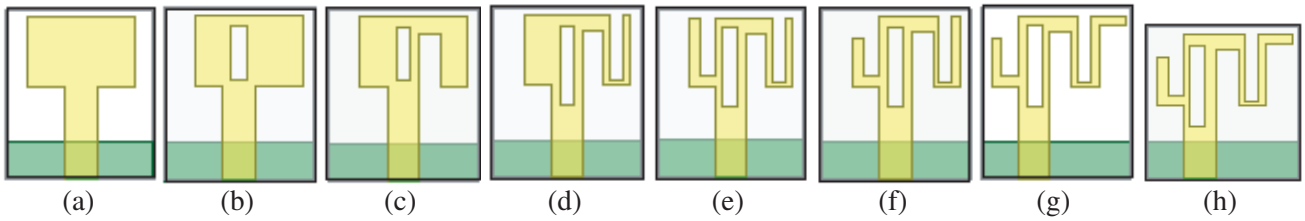

Figure 3. Evolution stages of antenna. (a) Antenna 1, (b) Antenna 2, (c) Antenna 3, (d) Antenna 4, (e) Antenna 5, (f) Antenna 6, (g) Antenna 7, (h) Antenna 8.

r [26].

$$L \times W = 2\pi r \times L$$
$$\therefore r = W/2\pi$$

The lowest frequency f_L of a wire antenna is given by

$$L + r = 0.24\lambda \text{ where } \lambda = c/f$$
$$L + r = 72/f_L \text{ where } L \text{ and } r \text{ are in mm and } f_L \text{ in GHz}$$
$$f_L = 72/(L + W/2\pi)$$

The gap 'g' between the radiating patch and ground plane increases the effective length of RMPA.

$$f_L = 72/(L + W/\pi + g)$$

However, the above equation does not consider the effect of substrate permittivity and thickness; therefore, a factor k is included in the above equation [27].

$$f_L = 72/(k \times (L + W/2\pi + g) \quad (1)$$

$k = 1.15$ for 1.6 mm FR4 substrate [26, 27]. The simulated f_L is 4.69 GHz which is close to calculated f_L using Equation (1) 4.61 GHz ($L = 6.6$ mm, $W = 10$ mm and $g = 5.4$ mm). RMPA, 'Antenna 1', resonates at 5.5 GHz and provides $S_{11} < -10$ dB from 4.69 to 6.53 GHz as shown in Fig. 4.

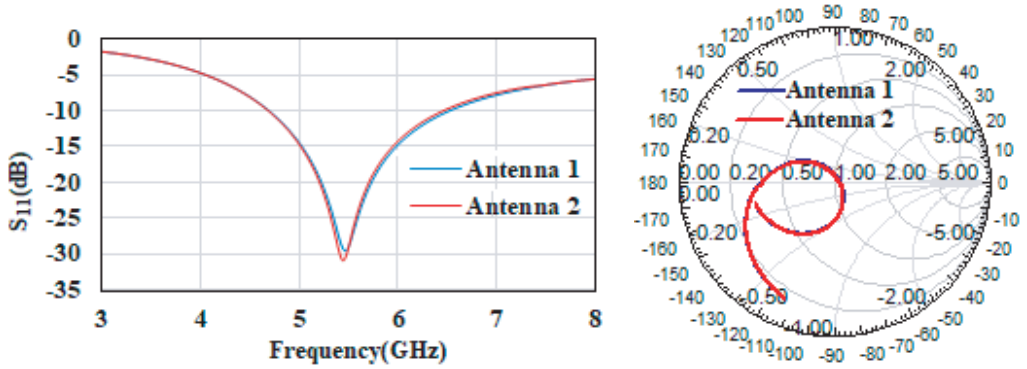

Figure 4. S_{11} and impedance variation of Antenna 1 and Antenna 2.

In 'Antenna 2', 'slot A' is etched, and a rectangular-shaped radiating patch is shifted towards right. Asymmetry is introduced so that the left part of the structure can be made to resonate over higher frequency band, and the right part resonates over lower frequency band in the subsequent stages. $S_{11} < -10$ dB is obtained from 4.68 to 6.46 GHz shown in Fig. 4. There is negligible change in impedance variation and resonant frequency as compared to Antenna 1. In 'Antenna 3', a 'slot B' is etched in the right part of 'Antenna 2', which increases the capacitance of the structure, and therefore, impedance plot shifts downwards as shown in Fig. 5. The slot results in two distinct current paths which give rise

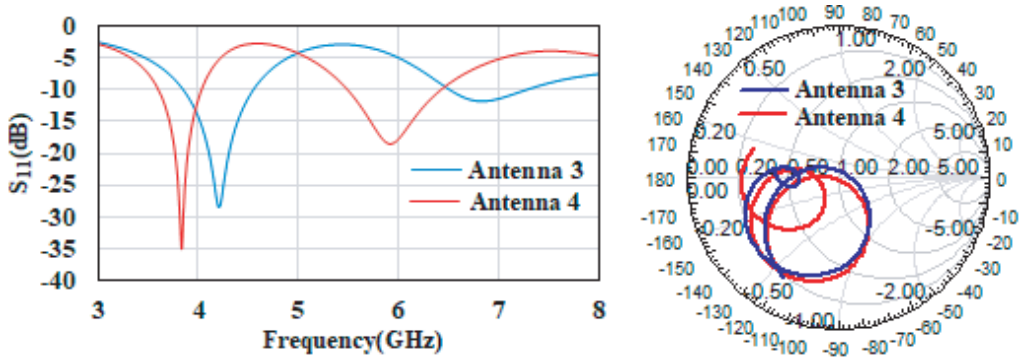

Figure 5. S_{11} and impedance variation of Antenna 3 and Antenna 4.

to a dual band antenna. $S_{11} < -10$ dB is obtained from 3.85 to 4.55 GHz and 6.5 to 7.28 GHz as shown in Fig. 5. However, the impedance matching is poor over the higher band. The lower band shifts to 3.85 from 4.55 GHz which corresponds to about 18% reduction in size or miniaturization of antenna.

Another 'slot C' is etched in 'Antenna 3' at the top on the right side of previous slot to form 'Antenna 4'. The slot increases the capacitance, and therefore, resonant frequencies of both the bands decrease. Impedance matching improves over the upper band. The impedance variation plot shifts downward. Two loops on the impedance plot indicate the dual band behavior of the structure as shown in Fig. 5. However, the capacitive effect of this slot is less than previous slot due to less surface current density, and therefore, the decrease in resonant frequency is less than the previous slot. $S_{11} < -10$ dB is obtained from 3.6 to 4.03 GHz and 5.5 to 6.43 GHz as shown in Fig. 5.

Now, a 'slot D' is etched oat the top in 'Antenna 4' on the left side of the feed line to form 'Antenna 5'. As the surface current density is less on this portion at lower band, when a slot is etched, it does not affect the lower band. However, there is appreciable surface current density on the left side of the structure at higher band; therefore, left side slot affects the upper band. The capacitance increases due to the slot, and therefore, impedance plot shifts downward. The emergence of third loop on the impedance plot indicates the tri-band behavior of the structure as shown in Fig. 6. However, impedance matching is poor over this band. $S_{11} < -10$ dB is obtained over 3.6 to 4.0 GHz and 5.35 to 6.1 GHz as shown in Fig. 6.

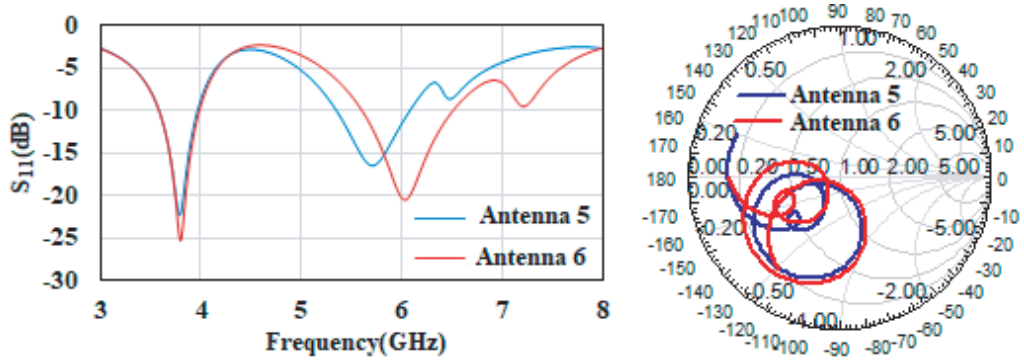

Figure 6. S_{11} and impedance variation of Antenna 5 and Antenna 6.

In 'Antenna 6', length of the left side arm is decreased. As surface current density is less on this portion at lower band, it does not affect the lower band, but the resonant frequencies of second and third bands increase. The impedance matching improves over the third band, but still, it is not satisfactory. The decrease in the length of left arm decreases the capacitance. As the capacitance decreases, the plot on impedance variation shifts upward as shown in Fig. 6. $S_{11} < -10$ dB is obtained from 3.6 to 4.0 GHz and 5.6 to 6.5 GHz as shown in Fig. 6.

In 'Antenna 7', an arm is added on the right side of 'Antenna 6', to operate the structure over 3.3–3.6 GHz for 5G applications. As path length increases, the resonant frequencies of lower and middle bands decrease. However, it degrades impedance matching over the upper band. $S_{11} < -10$ dB is obtained from 3.25 to 3.64 GHz and 5.55 to 6.1 GHz as shown in Fig. 7. The inductance of the structure increases due to introduction of this branch, and therefore, the impedance plot shifts upward as shown in Fig. 7.

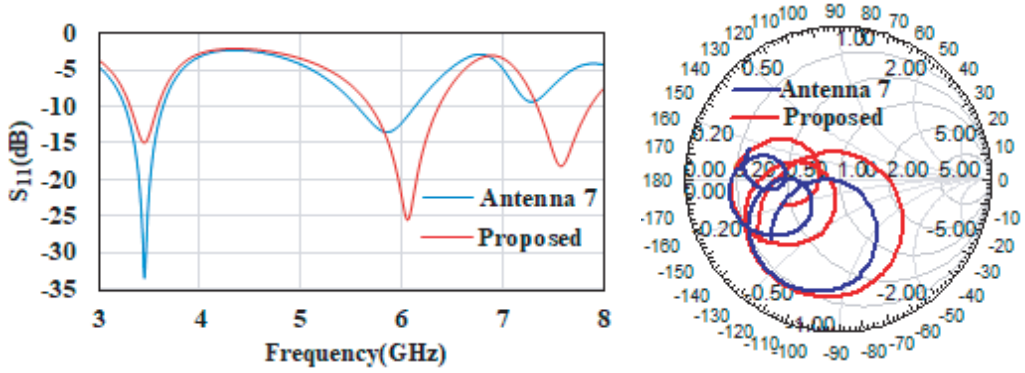

Figure 7. S_{11} and impedance variation of Antenna 7 and Proposed Antenna 8.

The structure is optimized to improve S_{11} and obtain the desired bands. The 'slot A' in the feed arm is shifted towards left, and the gap 'Pg' between antenna and ground plane is optimized. The proposed 'Antenna 8' operates over 3.3 to 3.6 GHz, 5.7 to 6.4 GHz, and 7.3 to 7.9 GHz as depicted in Fig. 7. The proposed 'Antenna 8' results in about 30% reduction in size or miniaturization as compared to Antenna 1. Further, 'Antenna 1' is designed on a $16 \times 14\,\text{mm}^2$ substrate while the substrate dimensions of proposed 'Antenna 8' are $14 \times 13\,\text{mm}^2$. The portion to the left of the antenna feed 'slot D' affects the upper band; the portion just right to the feed 'slot B' affects the lower band; and the portion right to it 'slot C' affects the middle band.

Parametric study is conducted on parameters that affect the bandwidth and resonant frequency of three bands. The length of the left side arm '$L1$' has negligible effect on lower band. Increase in the length of '$L1$' increases the capacitance. As the capacitance increases, resonant frequency of middle band decreases. However, it degrades the impedance matching at upper band. Return loss for different '$L1$' is shown in Fig. 8(a).

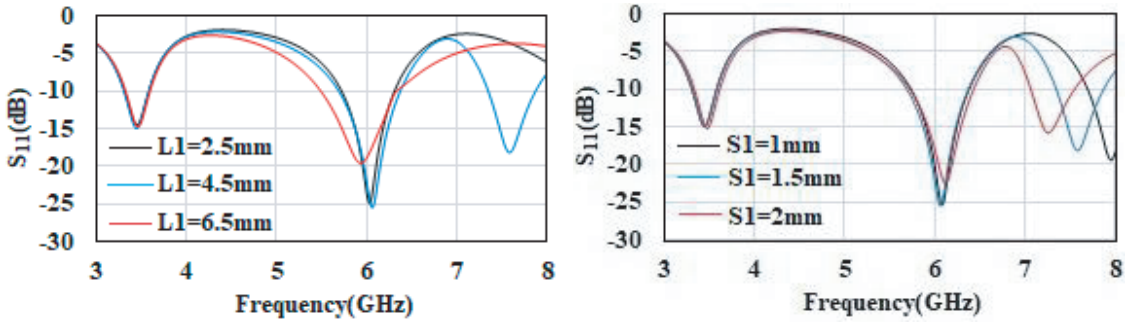

Figure 8. (a) Different $L1$, (b) different $S1$.

As '$S1$' decreases, the perimeter of left arm decreases, which decreases the current path length and inductance. Further, the decrease in '$S1$' increases the capacitance also. At the upper band, the surface current density is maximum on this arm; therefore, inductive effect dominates, and hence resonant frequency increases with the decrease in '$S1$' due to decrease in inductance. However, the inductive

effect decreases due to less surface current density over middle band, and capacitive effect dominates. Therefore, resonant frequency of middle band decreases with the decrease in '$S1$'. The increase in resonant frequency is more at upper band as the decrease in electric path length is more at higher frequency. As the surface current density is less on this portion at lower band, '$S1$' does not affect lower band. S_{11} for different '$S1$' is shown in Fig. 8(b).

As '$W2$' increases, the slot area and capacitance decrease; therefore, the resonant frequencies increase with the increase in '$W2$'. Since the surface current in the arms surrounding 'slot B' is maximum at the lower band and minimum at the upper band, the increase in '$W2$' increases the resonant frequency of lower band more than the middle and upper bands. S_{11} for different '$W2$' is shown in Fig. 9(a).

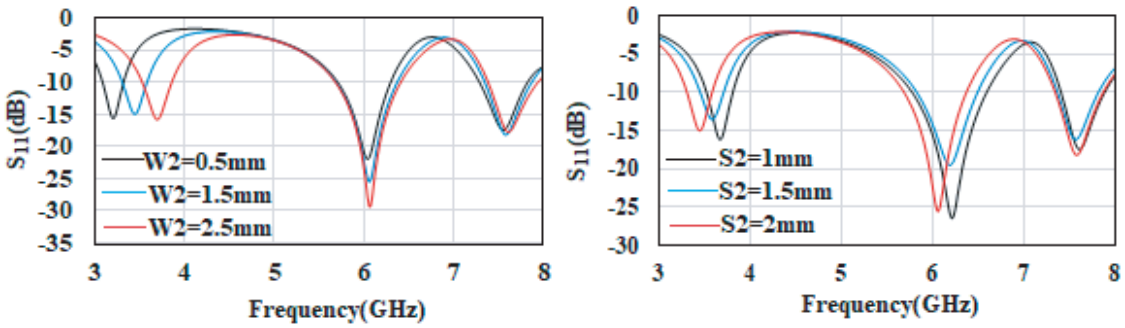

Figure 9. (a) Different $W2$, (b) different $S2$.

As '$S2$' decreases, the perimeter of arms surrounding the slot B near the feed line decreases, which decreases the path length and inductance. Therefore, resonant frequencies of bands increase with the decrease in '$S2$'. Since the surface current in the arm near feed line is maximum at lower band and minimum at upper band, the decrease in '$S2$' increases the resonant frequency of lower band more than the middle and upper bands. S_{11} for different '$S2$' is shown in Fig. 9(b).

As '$L3$' increases, the perimeter of arms surrounding the 'slot C' increases, which increases the path length and inductance. Therefore, resonant frequencies of bands decrease with the increase in '$L3$'. Since the surface current in the arms surrounding 'slot C' is maximum over the middle band and minimum over the upper band, the increase in '$L3$' decreases the resonant frequency of middle band more than the lower and upper bands. S_{11} for different '$L3$' is depicted in Fig. 10(a).

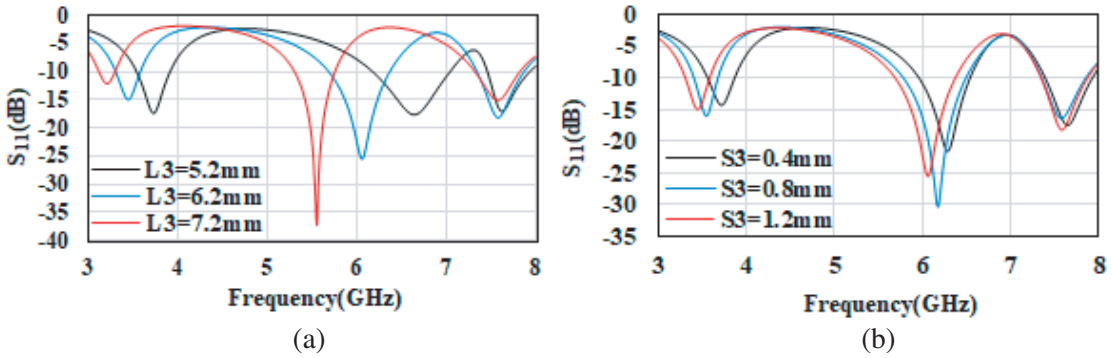

Figure 10. (a) Different $L3$, (b) different $S3$.

As '$S3$' increases, the perimeter of arms surrounding the 'slot C' increases, which increases the path length and inductance. Therefore, resonant frequencies of bands decrease with increase in '$S3$'. Since the surface current in the arms surrounding 'slot C' is maximum over the middle band and minimum over the upper band, the increase in '$S3$' decreases the resonant frequency of middle band more than

the lower and upper band. S_{11} for different '$S3$' is depicted in Fig. 10(b).

The gap 'Pg' acts as a matching network and plays a vital role in impedance matching of a monopole antenna. The space between ground plane and radiating element acts as a capacitor, while conducting strip is equivalent to an inductor. The optimum value of gap 'Pg' depends on the monopole structure. The return loss for different 'Pg' is shown in Fig. 11(a). The position of 'slot A' also affects the impedance matching. Therefore, 'w' is optimized to achieve the desired bands. S_{11} for different 'w' is shown in Fig. 11(b).

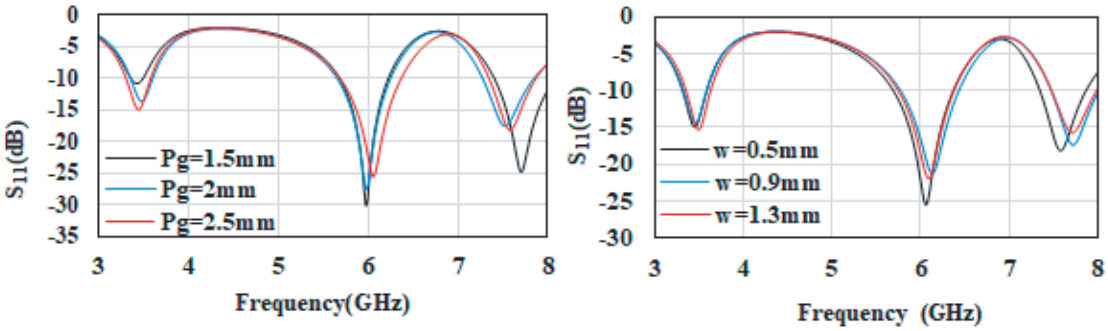

Figure 11. (a) different Pg, (b) different w.

The tri-band operation of the proposed 'Antenna 8' is investigated by analyzing surface current distribution. The surface current densities at 3.45 GHz, 6.0 GHz, and 7.6 GHz are shown in Fig. 12. At 3.45 GHz, the surface current density is mostly concentrated around 'slot B'. There is little surface current in the left side arm at 3.45 GHz; therefore, the change in dimensions of '$L1$' and '$S1$' has slight effect on lower band. Also dimensions of '$W2$' and '$S2$' have the maximum effect on lower band. The surface current density is mostly concentrated around 'slot C' at 6.0 GHz. Therefore, dimensions of '$L3$' and '$S3$' have the maximum effect on middle band. The surface current density is maximum around 'slot D' at 7.6 GHz; therefore, dimensions of '$L1$' and '$S1$' have the maximum effect on upper band. Thus, the dimensions of three slots control the three bands and can be optimized to achieve the desired bandwidth over the three bands.

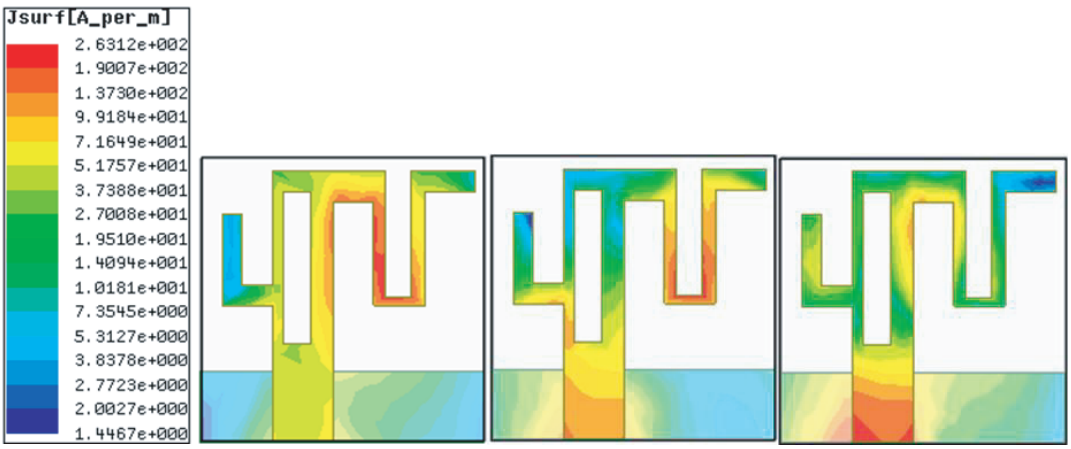

Figure 12. Surface current distribution of proposed antenna. (a) 3.45 GHz, (b) 6.0 GHz, (c) 7.6 GHz.

A miniaturized tri-band antenna is designed by etching slots in the RMPA. A slot, etched in an RMPA, results in the emergence of a band. Three slots are etched to provide the desired triple bands.

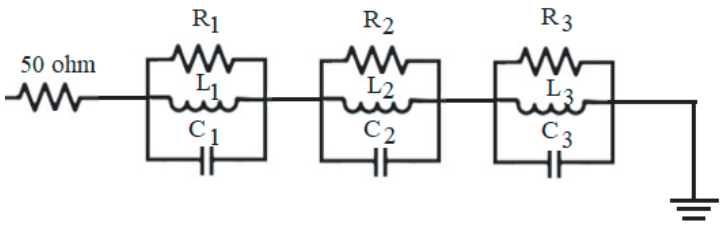

Figure 13. Equivalent circuit of proposed tri-band antenna [14].

The surface current distribution changes with the introduction of a slot, and it results in additional resonant frequency. The equivalent circuit of the designed tri-band antenna is shown in Fig. 13. Three parallel resonating circuits represent the three bands. Elements R_1, L_1, and C_1 represent the lower band and resonate at 3.45 GHz; elements R_2, L_2, and C_2 resonate at 6 GHz and represent the middle band while the elements R_3, L_3, and C_3 represent the upper band and resonate at 7.6 GHz. The value of these elements can be calculated using Equations (2)–(5) [14].

$$\omega_i = \pi f_i \tag{2}$$

$$fo_i = 1/\pi\sqrt{L_i C_i} \tag{3}$$

$$Q_i = fo_i/BW_i = \omega_i L_i/R_i \tag{4}$$

$$C_i = \varepsilon_0 \varepsilon_r Si/h \tag{5}$$

Here $i = 1, 2, 3$ for lower, middle, and upper bands, respectively. fo_i, ω_i, Q_i, and BW_i are resonant frequency, angular frequency, quality factor, and bandwidth of a band, respectively, whereas R_i, L_i, and C_i are the resistance, inductance, and capacitance of a band, respectively. ε_0, ε_r, and h represent the permittivity of free-space, dielectric constant, and thickness of the substrate, respectively. S_i is the surface area of that part of antenna that radiates over a band. Table 2 lists the values of various parameters and elements of the equivalent circuit, calculated using Equations (2)–(5) [14]. As radiating area S_i decreases with the increase in frequency, capacitance value decreases with frequency. The decrease in effective current path length results in the decrease in inductance with the increase in frequency.

Table 2. Values of elements of equivalent circuit of the proposed antenna.

Parameters	Lower band ($i = 1$)	Middle band ($i = 2$)	Upper band ($i = 3$)
Resonant frequency (f_{0i}) GHz	3.45	6.0	7.6
Band width (BW_i) GHz	0.3 GHz	0.7 GHz	0.6 GHz
Quality Factor (Q_i)	11.5	8.57	12.67
Resistance (R_i) Ω	49.3	48.7	41.4
Inductance (L_i) Nh	26.7	11.07	10.99
Capacitance (C_i) pf	0.081	0.064	0.04

3. FABRICATION AND MEASURED RESULTS

The proposed "Antenna 8' is fabricated, and its photograph is shown in Fig. 2. 9916A Agilent network analyzer is used for measuring S_{11}. Measured along with simulated S_{11} are shown in Fig. 14(a). Radiation patterns and gain are measured in an anechoic chamber using a standard horn antenna. The measured gain at distinct frequencies along with simulated gain is shown in Fig. 14(b). Peak gain of 1.5 dBi, 2.8 dBi, and 3.7 dBi is obtained over lower, middle, and upper bands, respectively with < 1 dB gain variation over each band. The radiation patterns shown in Fig. 15 are nearly omnidirectional. As evident from Fig. 12, significant current densities in horizontal and vertical arms around 'slot B', 'slot

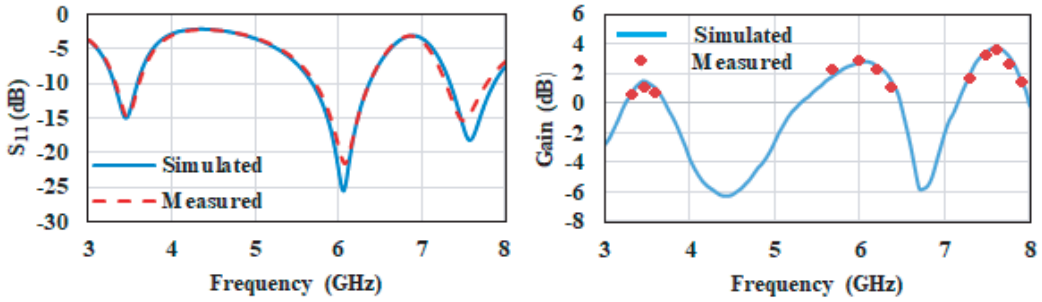

Figure 14. Measured and simulated results. (a) S_{11} vs. frequency, (b) gain vs. frequency.

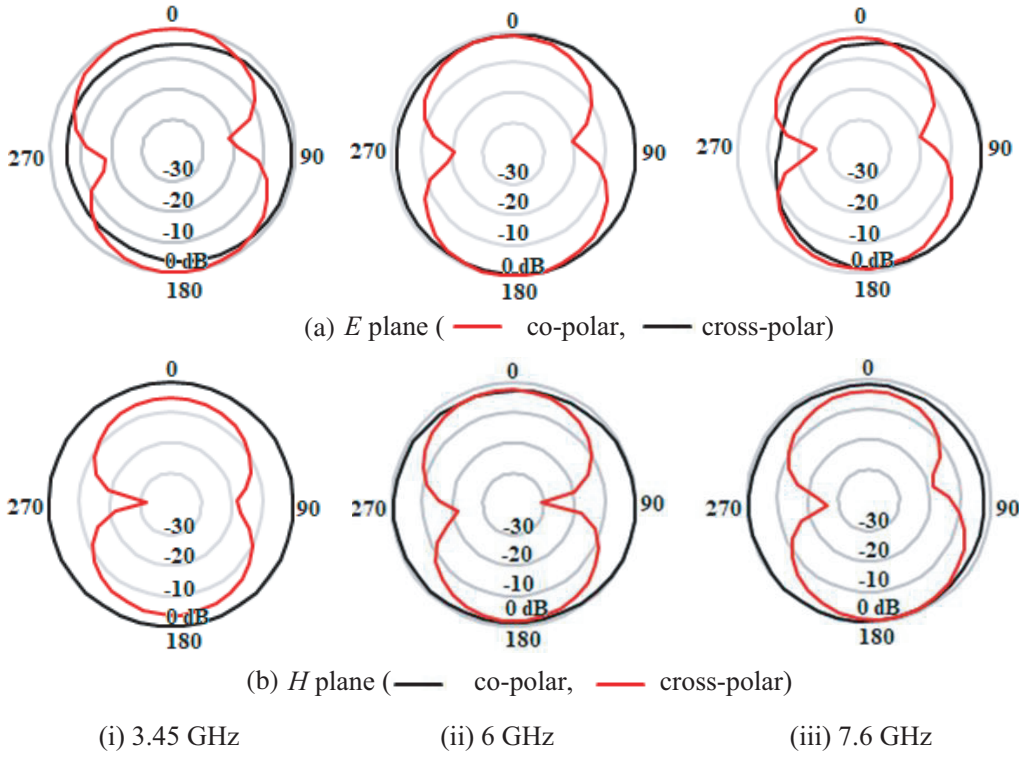

Figure 15. Radiation patterns of proposed antenna.

C', and 'slot D' at 3.45 GHz, 6.0 GHz, and 7.6 GHz, respectively, have resulted in high cross-polarization over the three bands.

4. COMPARISON WITH REPORTED ANTENNAS

The designed antenna is compared with reported antenna based on their dimensions and design techniques employed for obtaining tri-band in Table 3. The proposed antenna occupies less substrate area than the reported antennas except [17]. [17] has smaller dimensions than the proposed antenna, but it is difficult to fabricate and uses multiple substrates. Tri-band antennas in [1, 2] have multiple branches. Besides branches, slots and slits are etched, and stubs are added in [3–11] to obtain desired tri-bands. The antenna in [13] is designed using strips and SRR, and [14] is designed using SRR and half-split ring, while fractal technique is employed in [20]. [1–11, 13, 14, 20] not only have larger dimensions but also suffer from design complexity. The proposed tri-band antenna is miniaturized by etching slots in RMPA. The antenna is compact, easy to design, and low in cost.

Table 3. Comparison of proposed antenna with reported multiband antennas.

Ref.	Approach/Technique	Antenna Size (mm^2) Electric Size ($\lambda o \times \lambda o$)	Bands (GHz)	S_{11} min (dB)	Antenna Gain (dBi) % Efficiency
[1]	Meander-line and G-shape branches, defective ground structure (DGS) to improve impedance bandwidth	23×20 0.18×0.15 $= 0.027\lambda o^2$	2.39–2.52 3.3–4.47 5.15–6.0	−17 −40 −13	NA NA
[2]	Three C-shaped round stubs branches for tri-band operation	24×28 0.18×0.22 $= 0.039\lambda o^2$	2.34–2.55 3.39–3.69 5.5–6.0	−22 −17 −14	2.3/2.6/3.7 NA
[3]	Rectangular monopole with pi and L-shaped slots for tri-band operation	27.5×20 0.22×0.158 $= 0.0348\lambda o^2$	2.37–2.52, 3.35–3.9, 4.97–7.85	−27 −24 −20	3.9/4.1/3.8 90/87/75
[4]	Two arc-shaped branches and two stubs for tri-band operation	18×34.5 0.137×0.262 $= 0.036\lambda o^2$	2.28–2.57 5.0–6.27 7.11–7.96	−40 −25 −15	1.5/2.8/3.4 NA
[5]	Three branches, trapezoidal ground for tri-band operation	17×23.5 0.13×0.18 $= 0.0234\lambda o^2$	2.29–2.59 3.37–3.75 4.85–6.23	−28 −42 −32	2.1/2.3/3.2 NA
[6]	Pentagon radiating patch with hooked branches and vertical slot for tri-band operation	18×35 0.192×0.374 $= 0.072\lambda o^2$	3.2–4.1 5.1–5.9 7.3–8.9	−20 −22 −25	4/4.2/4.2 78/80/86
[7]	Multiple stubs embedded in DGS for tri-band operation	43×33 0.33×0.2 $= 0.083\lambda o^2$	2.28–3.10 3.52–4.10 5.05–6.00	−29 −20 −20	4.4/3.8/5.5 NA
[8]	Thin L-shaped strip added to circular branch and similar shaped parasitic strip, reduction of coupling between higher order modes for tri-band operation	32×21 0.224×0.147 $= 0.033\lambda o^2$	2.1–2.485 5.05–5.67 8.4–9.0	−14 −26 −15	1.6/2.4/3.8 NA
[9]	One I-shaped, two L-shaped and two annular-ring slots in rectangular patch and DGS for impedance matching	44×45 0.331×0.339 $= 0.112\lambda o^2$	2.257–2.523 3.455–3.655 4.012–4.262	−35 −30 −20	4.1/2.5/2.2 NA
[10]	U and H shaped slots in rectangular patch and DGS for tri-band operation	18×18 0.15×0.15 $= 0.0225\lambda o^2$	2.55–2.72 3.25–3.35 5.75–6.1	−14 −13 −15	0.2/0.16/0.62 68/56/72
[11]	SRR slot in rectangular monopole and U-shaped slot in ground	25×38 0.2×0.304 $= 0.0608\lambda o^2$	2.4–2.5 3.0–4.0 5.2–5.9	−21 −17 −19	1.9/2.0/2.1 NA
[13]	Slot antenna along with SRR and strips for tri-band operation	50×50 0.247×0.247 $= 0.061\lambda o^2$	1.48–1.87 2.39–2.71 3.02–3.16	−28 −24 −16	2.7/4.2/3.575 /90/82
[14]	SRR and half-split ring radiator for tri-band operation	32×22 0.24×0.165 $= 0.0396\lambda o^2$	2.25–2.55 3.6–3.99 5.5–6.4	−24 −33 −30	1.4/0.9/1.0 83/72/68
[17]	Two square and hexagon rings, multiple substrates for tri-band operation	60×4 0.176×0.117 $= 0.0206\lambda o^2$	0.88–1.03 1.47–2.74 3.32–5.97	−17 −33 −15	−0.2/3.6/4.4 66/87/88
[20]	Circular and triangular fractals for tri-band operation	87.5×61 0.525×0.366 $= 0.192\lambda o^2$	1.8–2.9 3.4–4.6 5–5.6	−27 −30 −15	2.9/2.6/3.3 92.5/75.5/95
This work	Slots in a rectangular monopole antenna for tri-band operation	14×13 0.154×0.143 $= 0.0220\lambda o^2$	3.3–3.6 5.7–6.4 7.3–7.9	−15 −25 −17	1.5/2.8/3.7 78/93/90

5. CONCLUSION

A novel miniaturized triband antenna by etching slots in an RMPA is proposed. The dimensions of three slots control the three bands which can be optimized to achieve the desired bandwidth over the three bands. The antenna operates over 3.3 to 3.6 GHz, 5.7 to 6.4 GHz, and 7.3 to 7.9 GHz. The antenna is simple to design and low in cost and offers omnidirectional radiation patterns with < 1 dB gain variation over each band. Thus, the designed antenna is suitable for 5G, WLAN, WiMAX, Cellular Vehicle-to-Everything (C-V2X) technology, and X-band applications.

REFERENCES

1. Zaman, W., H. Ahmad, and H. A. Mahmood, "Miniaturized meandered printed monopole antenna for triband applications," *Microwave and Optical Technology Letter*, Vol. 60, No. 5, 1265–1271, 2018.
2. Woo, D. S., "A triple band C-shape monopole antenna for vehicle communication application," *Progress In Electromagnetics Research C*, Vol. 121, 97–106, 2022.
3. Ahmad, H., W. Zaman, S. Bashir, and M. U. Rahman, "Compact triband slotted printed monopole antenna for WLAN and WiMAX applications," *Int. J. RF Microw. Comput. Aided Eng.*, Vol. 29, 2019.
4. Zhi, R., M. Han, J. Bai, W. Wu, and G. Liu, "Miniature multiband antenna for WLAN and X-band satellite," *Progress In Electromagnetics Research Letters*, Vol. 75, 13–18, 2018.
5. Osklang, P., C. Phongcharoenpanich, and P. Akkaraekthalin, "Triband compact printed antenna for 2.4/3.5/5 GHz WLAN/WiMAX applications," *International Journal of Antennas and Propagation*, Article ID 8094908, 2019.
6. Mallat, N. K. and A. Iqbal, "Multi-band printed antenna for portable wireless communication applications," *Progress In Electromagnetics Research Letters*, Vol. 84, 39–46, 2019.
7. Jing, J., J. Pang, H. Lin, Z. Qiu, and C. Liu, "A multiband compact low-profile planar antenna based on multiple resonant stubs," *Progress In Electromagnetics Research Letters*, Vol. 94, 1–7, 2020.
8. Khade, A., M. Trimukhe, S. Jagtap, and R. K. Gupta, "A circular sector with an inverted L shaped monopole antenna for tri-band applications," *Progress In Electromagnetics Research C*, Vol. 118, 177–186, 2022.
9. Maity, B. and S. K. Nayak, "Design of compact microstrip-fed triple-band slot antenna with defected ground structure for wireless communications," *Journal of Electromagnetic Waves and Applications*, Vol. 36, No. 12, 1702–1716, 2022.
10. Ali, T. and R. C. Biradar, "A triple-band highly miniaturized antenna for WiMAX/WLAN applications," *Microwave and Optical Technology Letter*, Vol. 60, No. 2, 466–471, 2018.
11. El Misilmani, H. M., M. Al-Husseini, K. Y. Kabalan, and A. El-Hajj, "A simple miniaturized triple-band antenna for WLAN/WiMAX applications," *PIERS Proceedings*, Moscow, Russia, August 19–23, 2012.
12. Banerjee, U., A. Karmakar, A. Saha, and P. Chakraborty, "A CPW-fed compact monopole antenna with defected ground structure and modified parasitic Hilbert strip having wideband circular polarization," *AEU — International Journal of Electronics and Communications*, Vol. 110, 152831, 2019, ISSN 1434-8411.
13. Paul, P. M., K. Kandasamy, and M. S. Sharawi, "A tri-band circularly polarized strip and SRR loaded slot antenna," *IEEE Transactions on Antennas and Propagation*, Vol. 66, No. 10, 5569–5573, 2018.
14. Abdulzahra, D. H., F. Alnahwi, A. S. Abdullah, Y. I. A. Al-Yasir, and R. A. Abd-Alhameed, "A miniaturized triple-band antenna based on square split ring for IoT applications," *Electronics*, 2–14, 2022.

15. Dhara, R. and M. Monojit, "A triple-band circularly polarized annular ring antenna with asymmetric ground plane for wireless applications," *Engineering Reports*, Vol. 2, No. 4, e12150, 2020.
16. Garg, P. and P. Jain, "Design and analysis of a metamaterial inspired dual band antenna for WLAN application," *International Journal of Microwave and Wireless Technologies*, Vol. 11, No. 4, 1–8, 2019.
17. Yazdani, R., M. Yousefi, H. Aliakbarian, H. Oraizi, and G. A. E. Vandenbosch, "Miniaturized triple-band highly transparent antenna," *IEEE Transactions on Antennas and Propagation*, Vol. 68, No. 2, 712–718, 2020.
18. Rajalakshmi, P. and N. Gunavathi, "Hexagonal split ring resonator enclosed circular split ring resonator inspired dual-band antenna for sub-6 GHz 5G NR and IEEE 802.11ba/be applications," *Progress In Electromagnetics Research C*, Vol. 115, 1–15, 2021.
19. Verulkar, S., A. Khade, M. Trimukhe, and R. K. Gupta, "Dual band split ring monopole antenna structures for 5G and WLAN applications," *Progress In Electromagnetics Research C*, Vol. 122, 17–30, 2022.
20. Wang, L., J. Yu, T. Xie, and K. Bi, "A novel multiband fractal antenna for wireless application," *International Journal of Antennas and Propagation*, Article ID 9926753, 2021.
21. Ran, X., Z. Yu, T. Xie, Y. Li, X. Wang, and P. Huang, "A novel dual-band binary branch fractal bionic antenna for mobile terminals," *International Journal of Antennas and Propagation*, Article ID 6109093, 2020.
22. Asadallah, F. A., J. Costantine, and Y. Tawk, "A multiband compact reconfigurable PIFA based on nested slots," *IEEE Antenna and Wireless Propagation Letters*, Vol. 17, 331–334, 2018.
23. Koduri, S., G. S. Rao, and M. N. V. S. S. Kumar, "A compact grounded asymmetric coplanar strip-Fed flexible multiband reconfigurable antenna for wireless applications," *IEEE Access*, Vol. 8, 194497–194507, 2020.
24. Ahmad, A., F. Arshad, S. I. Naqvi, Y, Amin, H. Tenhunen, and J. Loo, "Flexible and compact spiral-shaped frequency reconfigurable antenna for wireless applications," *IETE Journal of Research*, Vol. 66, No. 1, 2020.
25. Ganesh, S. and Y. K. Choukiker, "Dual band frequency tunable planar inverted-F antenna for mobile handheld devices," *Int. J. RF Microw. Comput. Aided Eng.*, Vol. 30, No. 5, 2020.
26. Kumar, G. and K. P. Ray, *Broadband Microstrip Antennas*, Artech House, Norwood, MA, 2003.
27. Ray, K. P., "Design aspects of printed monopole antennas for ultra-wide band applications, *International Journal of Antennas and Propagation*, Vol. 2008, 1–8, 2008.